

1 *Physics and Chemistry of Minerals*

2 <https://doi.org/10.1007/s00269-018-1015-5>

3 ***Revision\_1***

4  
5 **H-bonding in lazulite: A single-crystal neutron diffraction study at**  
6 **298 and 3 K**

7  
8 G. Diego Gatta, Pietro Vignola, Nicola Rotiroti and Martin Meven  
9

10 **Running title:** Neutron diffraction study of lazulite

11 **Abstract, Keywords**

12 **Introduction**

13 **Sample description and occurrence**

14 **Experimental methods**

15 **Results and Discussion**

16 **Acknowledgements**

17 **References**

18 **Figures/Tables**

19  
20  
21 **Corresponding author: G. Diego GATTA**

22 Dipartimento di Scienze della Terra, Università degli Studi di Milano

23 Via Botticelli 23, I-20133 Milano, Italy

24 Tel. +39 02 503 15607, Fax +39 02 503 15597, E-Mail: [diego.gatta@unimi.it](mailto:diego.gatta@unimi.it)

25  
26  
27  
28  
29 *Manuscript submitted to Physics and Chemistry of Minerals*

# H-bonding in lazulite: A single-crystal neutron diffraction study at 298 and 3 K

G. Diego Gatta<sup>1,2</sup>, Pietro Vignola<sup>3</sup>, Nicola Rotiroti<sup>1</sup> and Martin Meven<sup>4</sup>

<sup>1</sup>Dipartimento di Scienze della Terra, Università degli Studi di Milano,  
Via Botticelli 23, I-20133 Milano, Italy

<sup>2</sup>CNR-Istituto di Cristallografia, Via Amendola 122/O, I-70126 Bari, Italy

<sup>3</sup>CNR-Istituto per la Dinamica dei Processi Ambientali, via Botticelli 23, I-20133, Milano, Italy

<sup>4</sup>Institute of Crystallography, RWTH Aachen University, and Jülich Centre for Neutron Science (JCNS) at Heinz Maier-Leibnitz Zentrum (MLZ), Lichtenbergstraße 1, D-85747 Garching, Germany

## Abstract

The crystal structure and crystal chemistry of a lazulite from Crosscut Creek (Kulan Camp area, Dawson mining district, Yukon, Canada) was investigated by electron microprobe analysis in wavelength-dispersive mode (EMPA) and single-crystal neutron diffraction at 298 and 3 K. Its empirical formula, based on EMPA data, is:  $(\text{Mg}_{0.871}\text{Fe}_{0.127})_{\Sigma 0.998}\text{Al}_{2.030}(\text{P}_{1.985}\text{Ti}_{0.008}\text{Si}_{0.007}\text{O}_4)_2(\text{OH})_2$ . The neutron diffraction experiments at room and low  $T$  proved that the H-free structural model of lazulite previously reported, on the basis of X-ray structure refinement, is correct: the building unit of the lazulite structure consists of a group of three face-sharing (Al-octahedron)+(Mg,Fe-octahedron)+(Al-octahedron), connected to the adjacent one *via* a corner-shared OH-group and two corner-shared oxygen sites of the P-tetrahedron, to form a dense 3D-edifice. Only one crystallographically independent H site occurs in the structure of lazulite, forming a hydroxyl group with the O5 oxygen, with O5-H = 0.9997 Å at room temperature (corrected for *riding motion effect*). The H-bonding scheme in the structure of lazulite is now well defined: a bifurcated bonding scheme occurs with the O4 and O2 oxygen sites as *acceptors*. The two H-bonds are energetically different, as shown by their bonding geometry: the H-bond with the O2 site as *acceptor* is energetically more favorable, being O5-H...O2 = 152.67(9)°, O5...O2 = 3.014(1) Å and H...O2 = 2.114(1) Å, whereas that with O4 as *acceptor* is energetically more costly, being O5-H...O4 = 135.73(8)°, O5...O4 = 3.156(1) Å and H...O4 = 2.383(1) Å, at room temperature. No  $T$ -induced phase transition occurs within the  $T$ -range investigated. At low temperature, the O5-H...O2 bond is virtually identical to the room- $T$  one, whereas the effects of  $T$  on O5-H...O4 are more pronounced, with significant differences of the  $\text{O}_{\text{donor}}\cdots\text{O}_{\text{acceptor}}$  and  $\text{H}\cdots\text{O}_{\text{acceptor}}$  distances. The experimental findings of this study do not support the occurrence of  $\text{HPO}_4$  or  $\text{H}_2\text{PO}_4$  units into the structure of lazulite, recently reported on the basis of infrared and Raman spectra.

67 **Keywords:** Lazulite; phosphates; single-crystal neutron diffraction; crystal chemistry; hydrogen  
68 bonding.

69

## 70 **Introduction**

71 Lazulite,  $\text{MgAl}_2(\text{PO}_4)_2(\text{OH})_2$ , was described for the first time in the phosphate-bearing meta-  
72 quartzites at Freissnitzgraben (Krieglach, Styria, Austria) by Klaproth (1795). This phosphate belongs to  
73 the “lazulite group” and forms a series with its Fe-analogue scorzalite,  $\text{FeAl}_2(\text{PO}_4)_2(\text{OH})_2$  (Pecora and  
74 Fahey 1950). Lazulite occurs in metamorphic quartzites (phosphate-bearing quartzites), granitic  
75 pegmatites and low temperature hydrothermal veins in sedimentary or anchimetamorphic terranes.

76 Its crystal structure was solved in the  $P2_1/c$  space group, with unit-cell parameters  $a \sim 7.16\text{\AA}$ ,  $b$   
77  $\sim 7.26\text{\AA}$ ,  $c \sim 7.24\text{\AA}$ ,  $\beta \sim 120.7^\circ$ , by Lindberg and Christ (1959), using a specimen from Minas Gerais,  
78 Brazil. The anisotropic structural model was later refined by Giuseppetti and Tadini (1983) in the same  
79 space group, using a specimen from the Graves Mountains (Georgia, U.S.A.). Giuseppetti and Tadini  
80 (1983) provided also the potential coordinates of one independent H site (forming a hydroxyl group  
81 with O-H distances of about  $0.8\text{\AA}$ ). The structure models of Lindberg and Christ (1959) and  
82 Giuseppetti and Tadini (1983) are mutually consistent and show that the triple-groups of face-sharing  
83 (Al-octahedron)+(Mg,Fe-octahedron)+(Al-octahedron) are connected to the adjacent ones by a corner-  
84 shared OH-group and two corner-shared oxygen sites of the P-tetrahedron (Fig. 1). However, in a more  
85 recent paper, based on infrared and Raman investigations of lazulite, Frost et al. (2013) reported  
86 evidence of bending modes ascribed to tetrahedral  $\text{PO}_4$ ,  $\text{HPO}_4$  and  $\text{H}_2\text{PO}_4$  units. These experimental  
87 findings are not consistent with the structural model reported by Lindberg and Christ (1959) and  
88 Giuseppetti and Tadini (1983), in which  $\text{HPO}_4$  and  $\text{H}_2\text{PO}_4$  groups are supposed not to occur. In  
89 addition, on the basis of their data, Frost et al. (2013) concluded that the proton on the hydroxyl units is  
90 apparently very mobile, promoting the formation of the monohydrogen and dihydrogen phosphate  
91 units.

92 In order to answer to the open questions about the structure of lazulite, and in the framework of a  
93 long-term project on the crystal-chemistry of hydrous phosphates (*e.g.*, Gatta et al. 2013a, 2013b,  
94 2014a, 2014b, 2015; Rotiroti et al. 2016), we have reinvestigated the crystal chemistry of lazulite by  
95 electron microprobe analysis in wavelength-dispersive mode (EMPA) and single-crystal neutron  
96 diffraction, in order to provide: *i*) the reliable location of the proton site(s) and the real configuration of  
97 the OH-group(s), for a full description of the H-bonds; *ii*) the anisotropic displacement parameters of  
98 all the atomic sites, H-site(s) included. In order to reduce the thermal displacement of the H-sites, and  
99 to confirm or deny the assumption on the proton mobility reported by Frost et al. (2013), single-crystal  
100 neutron diffraction data were collected at room temperature (298 K) and at low temperature (3 K).

## 101 **Sample description and occurrence**

102 The crystal of lazulite used in this study belongs to the private collection of one of the  
103 authors (P.V., catalogue #1493) and comes from the Crosscut Creek (Kulan Camp area, Dawson  
104 mining district, Yukon, Canada). The crystal was taken from the surface of a druse (8 x 5 cm)  
105 representing a portion of the wall of a hydrothermally mineralized vein, with mineral association:  
106 lazulite + quartz + siderite. The phosphate rich clefts, in the Dawson mining district, are due to an  
107 unusual hydrothermal post-depositional history involving the whole Rapid Creek Formation  
108 (Robertson 1980, 1982). This complex sedimentary sequence, consisting of highly phosphatic  
109 ironstones, comprises (from the textural point of view) shales, mudstones, siltstones and sandstones.  
110 The phosphate mineral associations occur in the coarser layers as epigenetic fracture fillings in  
111 veins or vugs. Lazulite is part of a “complex vein”, bearing a Ca-rich mineral association of the first  
112 type (*i.e.*, quartz + siderite + lazulite + “apatite”; Robertson 1982). This association typically takes  
113 place in veins perpendicular to the bedding of the mudstone host. The veins are about 40 cm wide  
114 and up to 10 m long.

## 115 **Experimental methods**

116 Quantitative EMPA in wavelength-dispersive mode was obtained from a polished and  
117 carbon-coated section using a JEOL JXA-8200 microprobe at the Earth Sciences Department,  
118 University of Milano (ESD-UMI). The system was operated using an accelerating voltage of 15 kV,  
119 a beam current of 5 nA, a beam diameter of 5  $\mu\text{m}$ , and a counting time of 30 s on the peaks and 10 s  
120 on the backgrounds. **The following standards were used:** graffonite KF-16 for P, Fe, Mn, and Ca;  
121 grossular for Si and Al; K-feldspar for K; forsterite for Mg; omphacite for Na; ilmenite for Ti;  
122 realgar for As. **Na, K, Ca, Mn and As were below the detection limits.** The raw data were corrected  
123 for matrix effects using the protocol implemented in the JEOL suite of programs. The averaged  
124 composition of the lazulite used in this study is given in Table 1.

125  
126 A single crystal of lazulite, optically homogeneous and free of inclusions or defects under a  
127 transmitted-light polarizing microscope, was selected for the X-ray and neutron diffraction  
128 experiments. A small fragment (0.31 x 0.27 x 0.17 mm<sup>3</sup>) was first investigated by single-crystal X-  
129 ray diffraction. X-ray intensity data were collected at room temperature and up to  $2\theta_{\text{max}} \cong 74^\circ$  with  
130 a Xcalibur - Oxford Diffraction diffractometer at the ESD-UMI, equipped with a CCD,  
131 monochromatized Mo- $K\alpha$  radiation and operated at 50 kV and 30 mA. The X-ray data collection  
132 was performed with a combination of  $\varphi/\omega$  scans, step size of  $1^\circ$  and an exposure time of 5 s/frame.  
133 The intensity data were integrated and indexed using the computer program CrysAlisPRO (Rigaku  
134 2018). A total number of 8427 Bragg reflections, out of which 1062 were unique for symmetry

135 (Laue class:  $2/m$ ,  $R_{\text{int}} = 0.041$ ), gave a metrically monoclinic unit-cell with:  $a = 7.139(1)$  Å,  $b =$   
136  $7.288(1)$ ,  $c = 7.236(1)$ ,  $\beta = 120.33(2)^\circ$ , according to the experimental findings of Giuseppetti and  
137 Tadini (1983), and the reflection conditions suggested the space group  $P2_1/c$  as highly likely.

138 A larger fragment from the same crystal (2 x 2 x 3 mm) was then used for the  
139 monochromatic neutron diffraction experiments at room and low temperature, using the  
140 diffractometer HEiDi at the hot source (fast neutrons) of the neutron source FRM II of the Heinz  
141 Maier-Leibnitz-Zentrum (MLZ), Germany. The diffractometer was equipped with a  $^3\text{He}$  single  
142 counter detector for high sensitivity down to short wavelengths. Two set of diffraction data were  
143 first collected at room temperature: a first set of data was collected with a wavelength of the  
144 incident beam of  $1.171(1)$  Å (Ge-311 monochromator, Er foil to suppress  $\lambda/3$  contamination) up to  
145  $2\theta_{\text{max}} = 121^\circ$  ( $\sin(\theta)/\lambda = 0.74$  Å $^{-1}$ ); a second set of data was collected at higher  $\sin(\theta)/\lambda$  up to  $0.89$  Å $^{-1}$ ,  
146 with a wavelength of the incident beam of  $0.795(1)$  Å (Ge-422 monochromator, Er foil to  
147 suppress  $\lambda/2$  contamination). In total, 2783 reflections were collected up to  $d_{\text{min}} \sim 0.7$  Å (with  $-12 \leq$   
148  $h \leq +12$ ,  $-13 \leq k \leq +13$  and  $-12 \leq l \leq +12$ , Table 2), using pure  $\omega$ -scan and  $\omega$ - $2\theta$  scan strategy as  
149 reported in Table 2, out of which 1755 were unique for symmetry and 1452 with  $F_o > 4\sigma(F_o)$ .  
150 Integrated intensities were then corrected for the Lorentz effect; absorption correction was found to  
151 be negligible. After the corrections, the discrepancy factor among symmetry-related reflections  
152 (Laue class:  $2/m$ ) was  $R_{\text{int}} = 0.0371$  (Table 2).

153 Low-temperature diffraction data were collected with a wavelength of the incident beam of  
154  $0.795(1)$  Å. The sample was fixed on an aluminium pin (0.8 mm diameter) and mounted on a  
155 closed-cycle cryostat to reach a minimum temperature of 3.0 K ( $\pm 0.1$  K). A total number of 2047  
156 reflections were collected up to  $d_{\text{min}} \sim 0.7$  Å (with  $-11 \leq h \leq +11$ ,  $-11 \leq k \leq +11$  and  $-11 \leq l \leq +11$ ,  
157 Table 2), using a pure  $\omega$ -scan strategy, out of which 1292 were unique for symmetry and 986 with  
158  $F_o > 4\sigma(F_o)$ . After corrected for the Lorentz effect, the discrepancy factor among symmetry-related  
159 reflections (Laue class:  $2/m$ ) was  $R_{\text{int}} = 0.0303$  (Table 2). Further details pertaining to the neutron  
160 data collections, at room and low  $T$ , are given in Table 2.

161 For both the data collections (*i.e.*, room and low  $T$ ), the lattice was found to be metrically  
162 monoclinic, and the reflections conditions were consistent with the space group  $P2_1/c$ , as previously  
163 reported by Giuseppetti and Tadini (1983). The evolution of intensity and full-width-at-half-  
164 maximum of three selected Bragg reflections (*i.e.*, 00-6, 040 and -400) were followed between  
165 room and low  $T$  (Fig. 2), showing no evidence of phase transition within the  $T$ -range investigated.

166 Anisotropic crystal-structure refinements, based on the neutron data collected at room and low  
167  $T$ , were done in the space group  $P2_1/c$  using the SHELXL-97 software (Sheldrick 1997, 2008),  
168 starting from the H-free structure model of Giuseppetti and Tadini (1983), and using the neutron

169 scattering lengths of Mg, Fe, Al, P, O and H from Sears (1986). Secondary isotropic extinction  
170 effect was corrected according to the formalism of Larson (1967), as implemented in the SHELXL  
171 package. After a few cycles of refinement, convergence was achieved with one (unique) intense  
172 negative residual peak in the final difference-Fourier map of the nuclear density (Fig. 3), located at  
173 *ca.* 1 Å from the O5 site. Further cycles of refinement were then done with H site assigned to this  
174 peak (as H has a negative neutron scattering length, Sears 1986). Convergence was achieved after a  
175 few cycles of refinement, with all the principal mean-square atomic displacement parameters  
176 positive, including those for the H site. At the end of the refinement, the variance-covariance matrix  
177 showed no significant correlation among the refined variables. Further details pertaining to structure  
178 refinement strategy are given in Table 2. Atomic coordinates and displacement parameters are listed  
179 in Tables 3 and 4; selected interatomic distances and angles are given in Table 5.

180

181

## 182 **Results and Discussion**

183 The EMPA data of the lazulite sample used in this study confirms its ideal formula:  
184  $\text{MgAl}_2(\text{PO}_4)_2(\text{OH})_2$  (Pecora and Fahey 1950, Lindberg and Christ 1959). P (in tetrahedral  
185 coordination) is replaced by a very modest fraction of Ti and Si, Al (in octahedral configuration)  
186 does not show any substituent, and Mg is replaced by Fe (Table 1). The Mg *vs.* Fe substitution is  
187 expected, as lazulite (ideally  $\text{MgAl}_2(\text{PO}_4)_2(\text{OH})_2$ ) and scorzalite (ideally  $\text{FeAl}_2(\text{PO}_4)_2(\text{OH})_2$ ) are  
188 supposed to form a complete isomorphous series (Pecora and Fahey 1950; Gheith 1953). The  
189 empirical formula of lazulite from Crosscut Creek used in this study is:  
190  $(\text{Mg}_{0.871}\text{Fe}_{0.127})_{\Sigma 0.998}\text{Al}_{2.030}(\text{P}_{1.985}\text{Ti}_{0.008}\text{Si}_{0.007}\text{O}_4)_2(\text{OH})_2$  (Table 1).

191 The neutron structure refinements of this study, based on intensity data collected at 298 and 3  
192 K, provide a general structural model of lazulite consistent with those previously reported by  
193 Lindberg and Christ (1959) and Giuseppetti and Tadini (1983), based on single-crystal X-ray  
194 intensity data collected at room **temperature**: the building unit of the lazulite structure consists of a  
195 group of three face-sharing (Al-octahedron)+(Mg,Fe-octahedron)+(Al-octahedron), connected to  
196 the adjacent one *via* a corner-shared OH-group and two corner-shared oxygen sites of the P-  
197 tetrahedron, to form a dense 3D-edifice (Fig. 1). The P-tetrahedron is the most regular coordination  
198 polyhedron [with  $\Delta(\text{P-O})_{\text{max}} \sim 0.03$  Å, *i.e.*, the difference between the longest and the shortest bond  
199 distances], the (Mg,Fe)-octehedron is slightly more distorted [ $\Delta(\text{Mg,Fe-O})_{\text{max}} \sim 0.06$  Å], whereas  
200 the Al-octahedron is strongly deformed [ $\Delta(\text{Al-O})_{\text{max}} \sim 0.20$  Å]. Only one crystallographically  
201 independent H site occurs in the structure of lazulite, forming a hydroxyl group with the O5 oxygen,  
202 with  $\text{O5-H}^* = 0.9997$  Å at room **temperature** (\*corrected for *riding motion effect*, Table 5). The H-

203 bonding scheme in the structure of lazulite is now well defined: a bifurcated bonding scheme occurs  
204 with the O4 and O2 oxygen sites as *acceptors* (Table 5). The two H-bonds are energetically  
205 different, as shown by their bonding geometry: the H-bond with the O2 site as *acceptor* is  
206 energetically more favorable, being  $O5-H\cdots O2 = 152.67(9)^\circ$ ,  $O5\cdots O2 = 3.014(1) \text{ \AA}$  and  $H\cdots O2 =$   
207  $2.114(1) \text{ \AA}$ , whereas that with O4 as *acceptor* is energetically more costly, being  $O5-H\cdots O4 =$   
208  $135.73(8)^\circ$ ,  $O5\cdots O4 = 3.156(1) \text{ \AA}$  and  $H\cdots O4 = 2.383(1) \text{ \AA}$ , at room **temperature**. At low  
209 temperature, the  $O5-H\cdots O2$  bond is virtually identical to the room- $T$  one (differences are within  
210  $0.001 \text{ \AA}$  and  $0.1^\circ$ , Table 5), whereas the effects of  $T$  on  $O5-H\cdots O4$  are more pronounced, with  
211 significant differences of the  $O_{\text{donor}}\cdots O_{\text{acceptor}}$  and  $H\cdots O_{\text{acceptor}}$  distances (*i.e.*,  $\sim 0.02 \text{ \AA}$ , Table 5).

212 The H-bonding scheme in the structure of lazulite here described is compatible with the  
213 findings based on infrared and Raman spectroscopies (*e.g.*, Frost et al. 2013, RRUFF database:  
214 <http://rruff.info/Lazulite>), as IR and Raman spectra, in the region of the OH stretching active modes,  
215 show evidence of more than one unique H-bond. The description of the IR and Raman mode in  
216 lazulite provided by Frost et al. (2013) is likely affected by misinterpretation: the structure does not  
217 contain  $HPO_4$  or  $H_2PO_4$  units, and, in addition, the conclusion “*The proton on the hydroxyl units is*  
218 *apparently very mobile and enables the formation of the monohydrogen and dihydrogen phosphate*  
219 *units*” (Frost et al. 2013) is inconsistent with our experimental findings and, in general, not  
220 plausible. We expect that a more robust description of the active IR and Raman vibrational modes  
221 will be delivered on the basis of the structure models of this study.

222 As shown by the root-mean-square components of the displacement ellipsoids at room  $T$   
223 (Table 4), the H site has the largest anisotropic displacement parameters, followed by the oxygen  
224 sites and then by the cationic sites. However, the disordered (Mg,Fe) site shows the largest  
225 displacement parameters among the cationic sites (*i.e.*, Mg-Fe, Al and P, Table 4). At low  $T$ , there is  
226 a general reduction of magnitude of the atomic displacement ellipsoids (by 10-40%), but not of their  
227 ellipticity ratio (Fig. 4, Table 4).

228 The Mg *vs.* Fe distribution is supposed not to change (at a significant level) between room  
229 and low  $T$ , as the mechanisms that promote intra-crystalline disordering, in this class of materials,  
230 are usually activated at high  $T$ . The slight difference between the refined Mg *vs.* Fe fraction at the  
231 octahedral site at room and low  $T$  are within  $3\sigma$  (Table 3), and therefore not significant. On the  
232 average, we can assume that the chemical formula of lazulite based on the neutron structure  
233 refinements is  $(Mg_{0.88(2)}Fe_{0.12(2)})Al_2(PO_4)_2(OH)_2$  (Table 3), in excellent agreement with the EMPA  
234 data.

235  
236

237 **Acknowledgements**

238 The authors acknowledge the Heinz Maier-Leibnitz Zentrum (MLZ) in Garching, Germany, for the  
239 allocation of neutron beam time at the single-crystal diffractometer HEIDI, operated by RWTH  
240 Aachen University and Jülich Centre for Neutron Science, Forschungszentrum Jülich (JARA  
241 cooperation). GDG and NR acknowledge the support of the Italian Ministry of Education (MIUR)  
242 through the project “Dipartimenti di Eccellenza 2018-2022”. E. Schingaro and an anonymous  
243 reviewer are thanked.

244

245

246 **References**

247 Busing WR, Levy HA (1964) The effect of thermal motion on the estimation of bond lengths from  
248 diffraction measurements. *Acta Crystallogr* 17:142-146.

249 Frost RL, Xi Y, Beganovic M, Belotti FM, Scholz R (2013) Vibrational spectroscopy of the  
250 phosphate mineral lazulite –  $(\text{Mg,Fe})\text{Al}_2(\text{PO}_4)_2(\text{OH})_2$  found in the Minas Gerais, Brazil.  
251 *Spectrochim Acta Part A (Molecular and Biomolecular Spectroscopy)* 107:241-247.

252 Gatta GD, Vignola P, Meven M, Rinaldi R (2013a) Neutron diffraction in gemology: Single-crystal  
253 diffraction study of brazilianite,  $\text{NaAl}_3(\text{PO}_4)_2(\text{OH})_4$ . *Am Mineral* 98:1624–1630.

254 Gatta GD, Nénert G, Vignola P (2013b) Coexisting hydroxyl groups and  $\text{H}_2\text{O}$  molecules in  
255 minerals: A single-crystal neutron diffraction study of eosphorite,  $\text{MnAlPO}_4(\text{OH})_2 \cdot \text{H}_2\text{O}$ . *Am*  
256 *Mineral* 98:1297–1301.

257 Gatta GD, Jacobsen SD, Vignola P, McIntyre GJ, Guastella G, Abate LF (2014a) Single-crystal  
258 neutron diffraction and Raman spectroscopic study of hydroxylherderite,  $\text{CaBePO}_4(\text{OH},\text{F})$ .  
259 *Mineral Mag*, 78, 723-737.

260 Gatta GD, Vignola P, Meven M (2014b) On the complex H-bonding network in paravauxite,  
261  $\text{Fe}^{2+}\text{Al}_2(\text{PO}_4)_2(\text{OH})_2 \cdot 8\text{H}_2\text{O}$ : A single-crystal neutron diffraction study. *Mineral Mag* 78:841–  
262 850.

263 Gatta GD, Redhammer GJ, Vignola P, Meven M, McIntyre GJ (2015) Single-crystal neutron  
264 diffraction and Mössbauer spectroscopic study of hureaulite,  $(\text{Mn,Fe})_5(\text{PO}_4)_2(\text{HPO}_4)_2(\text{H}_2\text{O})_4$ .  
265 *Eur J Mineral* 28:93-103.

266 Gatta GD, Rotiroti N, Cámara F, Meven M (2018) On the labyrinthine world of arsenites: a single-  
267 crystal neutron and X-ray diffraction study of cafarsite. *Phys Chem Minerals* 45:819–829.

268 Gheith MA (1953) Lipscombite: a new synthetic "iron lazulite". *Am Mineral* 38:612-628.

269 Giuseppetti G, Tadini C (1983) Lazulite,  $(\text{Mg,Fe})\text{Al}_2(\text{OH})_2(\text{PO}_4)_2$ , structure refinement and hydrogen  
270 bonding. *Neu Jb Mineral Mh.* 1983:410-416.



271 Klaproth MH (1795) Beiträge zur chemischen Kenntnis der Mineralkörper (first edition), Heinrich  
272 August Rottman, Berlin.

273 Larson AC (1967) Inclusion of secondary extinction in least-squares calculations. Acta Crystallogr  
274 23:664 – 665.

275 Lindberg LM, Christ CL (1959) Crystal structures of the isostructural minerals lazulite, scorzalite and  
276 barbosalite. Acta Crystallogr 12:695-697.

277 Pecora WT, Fahey JJ (1950) The lazulite-scorzalite isomorphous series. Am Mineral 35:1-18.

278 Rigaku (2018) CrysAlisPRO, computer suite. Rigaku Oxford Diffraction.

279 Robertson BT (1980) Stratigraphic setting of some new and rare phosphate minerals in the Yukon  
280 Territory. M.Sc. Thesis, University of Saskatchewan, Saskatoon, Canada.

281 Robertson BT (1982) Occurrence of epigenetic phosphate minerals in a phosphatic iron-formation,  
282 Yukon Territory. Can Mineral 20:177-187.

283 Rotiroti N, Vignola P, Bersani D, Simmons WB, Falster AU, Whitmore RW, Nizamoff J, Lotti P,  
284 Risplendente A, Pavese A (2016) On the crystal-chemistry of bjarebyite,  
285  $BaMn^{2+}_2Al_2(PO_4)_3(OH)_3$ , from the Palermo #1 pegmatite, Grafton County, New Hampshire,  
286 USA. Can Mineral 54:1033-1041.

287 Sears VF (1986) Neutron Scattering Lengths and Cross-Sections. In K. Sköld and D.L. Price, Eds.,  
288 Neutron Scattering, Methods of Experimental Physics, Vol. 23A, 521-550. Academic Press,  
289 New York.

290 Sheldrick GM (1997) SHELXL-97. Programs for crystal structure determination and refinement.  
291 University of Göttingen, Germany.

292 Sheldrick GM (2008) A short history of SHELX. Acta Crystallogr A64:112-122.

293

294

295 Table 1. EMPA chemical analysis of lazulite from Crosscut Creek (Kulan Camp area, Dawson  
 296 mining district, Yukon, Canada). Average composition based on 9 point-analysis.  
 297

298

	<i>wt %</i>	<i>e.s.d.</i>		<i>*a.p.f.u.</i>
P <sub>2</sub> O <sub>5</sub>	45.61	0.20	P	1.985 <sup>299</sup>
SiO <sub>2</sub>	0.13	0.05	Si	0.007
TiO <sub>2</sub>	0.21	0.10	Ti	0.008 <sup>301</sup>
Al <sub>2</sub> O <sub>3</sub>	33.51	0.18	sum	2.000 <sup>302</sup>
FeO	2.96	0.18		
MgO	11.37	0.12	Al	2.030 <sup>303</sup>
H <sub>2</sub> O**	5.83	0.03		
Total	99.63		Fe	0.127 <sup>304</sup>
			Mg	0.870 <sup>305</sup>
			sum	0.998 <sup>306</sup>
			H**	2.000 <sup>307</sup>

Notes: \*calculated on the basis of 2 (P+Si+Ti) a.p.f.u.; \*\* calculated on the basis of 2 OH-groups.

309

310

311 Table 2. Details of neutron data collections and refinements of lazulite.

312

313

314

315

316

317

318

319

320

321

322

323

324

325

326

327

328

329

330

331

332

333

334

335

336

337

338

$T$ (K)	298	3
Crystal shape	Prism	Prism
Crystal volume (mm)	2 x 2 x 3	2 x 2 x 3
Unit-cell parameters	$a = 7.139(1) \text{ \AA}$	$a = 7.137(1) \text{ \AA}$
	$b = 7.288(1) \text{ \AA}$	$b = 7.249(1) \text{ \AA}$
	$c = 7.236(1) \text{ \AA}$	$c = 7.201(1) \text{ \AA}$
	$\beta = 120.33(2)^\circ$	$\beta = 120.38(5)^\circ$
Reference chemical formula	$\text{MgAl}_2(\text{PO}_4)_2(\text{OH})_2$	$\text{MgAl}_2(\text{PO}_4)_2(\text{OH})_2$
Space Group	$P2_1/c$	$P2_1/c$
$Z$	2	2
Radiation type	neutron	neutron
Wavelength ( $\text{\AA}$ )	1.171(1), 0.795(1)	0.795(1)
Diffractometer	HEiDi-4circle	HEiDi-4circle
Data-collection method	$\omega$ -scan, $\omega$ -2 $\theta$ scan	$\omega$ -scan
$d_{\min}$ ( $\text{\AA}$ )	$\sim 0.7$	$\sim 0.7$
	$-12 \leq h \leq +12$	$-11 \leq h \leq +11$
	$-13 \leq k \leq +13$	$-11 \leq k \leq +11$
	$-12 \leq l \leq +12$	$-11 \leq l \leq +11$
Measured reflections	2783	2047
Unique reflections	1755	1292
Unique reflections with $F_o > 4\sigma(F_o)$	1452	986
Refined parameters	82	81
$R_{\text{int}}$	0.0371	0.0303
$R_\sigma$	0.0381	0.0407
$R_1(F)$ with $F_o > 4\sigma(F_o)$	0.0328	0.0293
$R_1(F)$ for all reflections	0.0580	0.0528
$wR_2(F^2)$	0.0578	0.0454
GooF	1.627	1.291
Residuals ( $\text{fm/\AA}^3$ )	-0.9/+0.8	-0.7/+0.6

Note: Statistical parameters according to the Shelxl-97 definition (Sheldrick 1997, 2008). Unit-cell parameters at room  $T$  based on single-crystal X-ray diffraction data. Further details pertaining to the data collection protocols are in Gatta et al. (2018).

339 Table 3. Refined fractional atomic coordinates and equivalent/isotropic displacement factors ( $\text{\AA}^2$ ),  
 340 based on the neutron structure refinements of lazulite at 298 and 3 K.  $U_{eq}$  is defined as one-third of  
 341 the trace of the orthogonalised  $U_{ij}$  tensor.  
 342  
 343

<i>Site</i>	<i>s.o.f.</i>	<i>x/a</i>	<i>y/b</i>	<i>z/c</i>	$U_{eq}$
<i>298 K</i>					
Mg	Mg 0.895(5), Fe 0.105(5)	0	0	0	0.00775(13)
Al	Al 1	-0.26734(8)	0.26678(8)	0.00630(10)	0.00574(10)
P	P 1	0.24810(6)	0.38541(5)	0.24507(7)	0.00544(8)
O1	O 1	-0.21236(6)	0.01394(5)	0.10605(7)	0.00877(8)
O2	O 1	-0.28791(6)	0.49997(5)	-0.09320(7)	0.00973(8)
O3	O 1	0.04396(5)	0.26401(5)	0.12474(6)	0.00873(8)
O4	O 1	-0.56186(5)	0.24243(6)	-0.12910(6)	0.00948(8)
O5	O 1	-0.26002(6)	0.14638(5)	-0.24144(6)	0.00735(8)
H	H 1	-0.38416(14)	0.06336(13)	-0.30098(15)	0.02493(18)
<i>3 K</i>					
Mg	Mg 0.876(7), Fe 0.124(7)	0	0	0	0.00288(17)
Al	Al 1	-0.26714(13)	0.26665(11)	0.00617(14)	0.00212(13)
P	P 1	0.24796(9)	0.38489(7)	0.24490(9)	0.00209(8)
O1	O 1	-0.21312(8)	0.01366(7)	0.10528(8)	0.00330(9)
O2	O 1	-0.28733(8)	0.50023(7)	-0.09256(8)	0.00351(9)
O3	O 1	0.04361(8)	0.26334(7)	0.12493(8)	0.00339(9)
O4	O 1	-0.56178(8)	0.24354(7)	-0.12952(8)	0.00351(9)
O5	O 1	-0.25998(9)	0.14669(7)	-0.24130(9)	0.00317(9)
H	H 1	-0.38447(18)	0.06335(16)	-0.30080(19)	0.0181(2)

344

345 Table 4. Refined displacement parameters ( $\text{\AA}^2$ ) in the expression:  $-2\pi^2[(ha^*)^2U_{11} + \dots + 2hka^*b^*U_{12}$   
 346  $+ \dots + 2klb^*c^*U_{23}]$  and root-mean-square displacement amplitude (*RMS*,  $\text{\AA}$ ), based on the neutron  
 347 structure refinements of lazulite at 298 and 3 K.  
 348

	$U_{11}$	$U_{22}$	$U_{33}$	$U_{12}$	$U_{13}$	$U_{23}$	<i>RMS-</i> <i>min</i>	<i>RMS-</i> <i>mid</i>	<i>RMS-</i> <i>max</i>	<i>max/min</i>
<i>298 K</i>										
Mg	0.0085(2)	0.0065(2)	0.0097(2)	0.0017(1)	0.0056(2)	0.0006(2)	0.0714	0.0888	0.1013	1.42
Al	0.0055(2)	0.0057(2)	0.0057(2)	0.0001(1)	0.0026(2)	0.0002(2)	0.0732	0.0753	0.0786	1.07
P	0.0054(1)	0.0051(1)	0.0057(1)	-0.0002(1)	0.0027(1)	-0.0001(1)	0.0709	0.0739	0.0764	1.08
O1	0.0115(1)	0.0075(1)	0.0098(2)	0.0017(1)	0.0072(1)	0.0024(1)	0.0752	0.0880	0.1138	1.51
O2	0.0149(2)	0.0068(1)	0.0108(2)	0.0008(1)	0.0090(1)	0.0018(1)	0.0734	0.0916	0.1241	1.69
O3	0.0058(1)	0.0082(1)	0.0104(2)	-0.0011(1)	0.0028(1)	-0.0024(1)	0.0722	0.0886	0.1145	1.58
O4	0.0061(1)	0.0101(1)	0.0107(2)	-0.0017(1)	0.0032(1)	-0.0028(1)	0.0737	0.0962	0.1173	1.59
O5	0.0083(1)	0.0074(1)	0.0061(1)	-0.0006(1)	0.0034(1)	0.0001(1)	0.0777	0.0842	0.0944	1.22
H	0.0250(3)	0.0285(4)	0.0202(4)	-0.0140(3)	0.0106(3)	-0.0057(3)	0.1122	0.1448	0.2031	1.81
<i>3 K</i>										
Mg	0.0037(3)	0.0024(3)	0.0030(3)	0.0006(2)	0.0020(2)	0.0001(2)	0.0446	0.0523	0.0625	1.40
Al	0.0030(3)	0.0018(3)	0.0020(3)	-0.0001(2)	0.0016(2)	0.0001(2)	0.0380	0.0438	0.0547	1.44
P	0.0025(2)	0.0018(2)	0.0021(2)	-0.0001(2)	0.0013(1)	-0.0003(2)	0.0390	0.0468	0.0505	1.29
O1	0.0047(2)	0.0027(2)	0.0035(2)	0.0002(2)	0.0029(2)	0.0011(2)	0.0374	0.0593	0.0704	1.88
O2	0.0055(2)	0.0023(2)	0.0038(2)	0.0001(2)	0.0033(2)	0.0007(2)	0.0413	0.0562	0.0751	1.82
O3	0.0031(2)	0.0029(2)	0.0038(2)	-0.0009(2)	0.0015(2)	-0.0008(1)	0.0449	0.0620	0.0657	1.46
O4	0.0030(2)	0.0036(2)	0.0037(2)	-0.0007(1)	0.0015(2)	-0.0010(1)	0.0490	0.0589	0.0683	1.39
O5	0.0042(2)	0.0031(2)	0.0027(2)	-0.0003(1)	0.0020(1)	0.0001(1)	0.0470	0.0552	0.0652	1.39
H	0.0179(4)	0.0192(5)	0.0164(4)	-0.0108(4)	0.0081(4)	-0.0043(3)	0.0880	0.1301	0.1719	1.95

351  
 352  
 353  
 354  
 355  
 356  
 357  
 358  
 359  
 360  
 361  
 362  
 363  
 364  
 365  
 366

367 Table 5. Relevant bond distances (Å) and angles (°) based on the neutron structure refinements at  
 368 298 and 3 K.  
 369  
 370  
 371

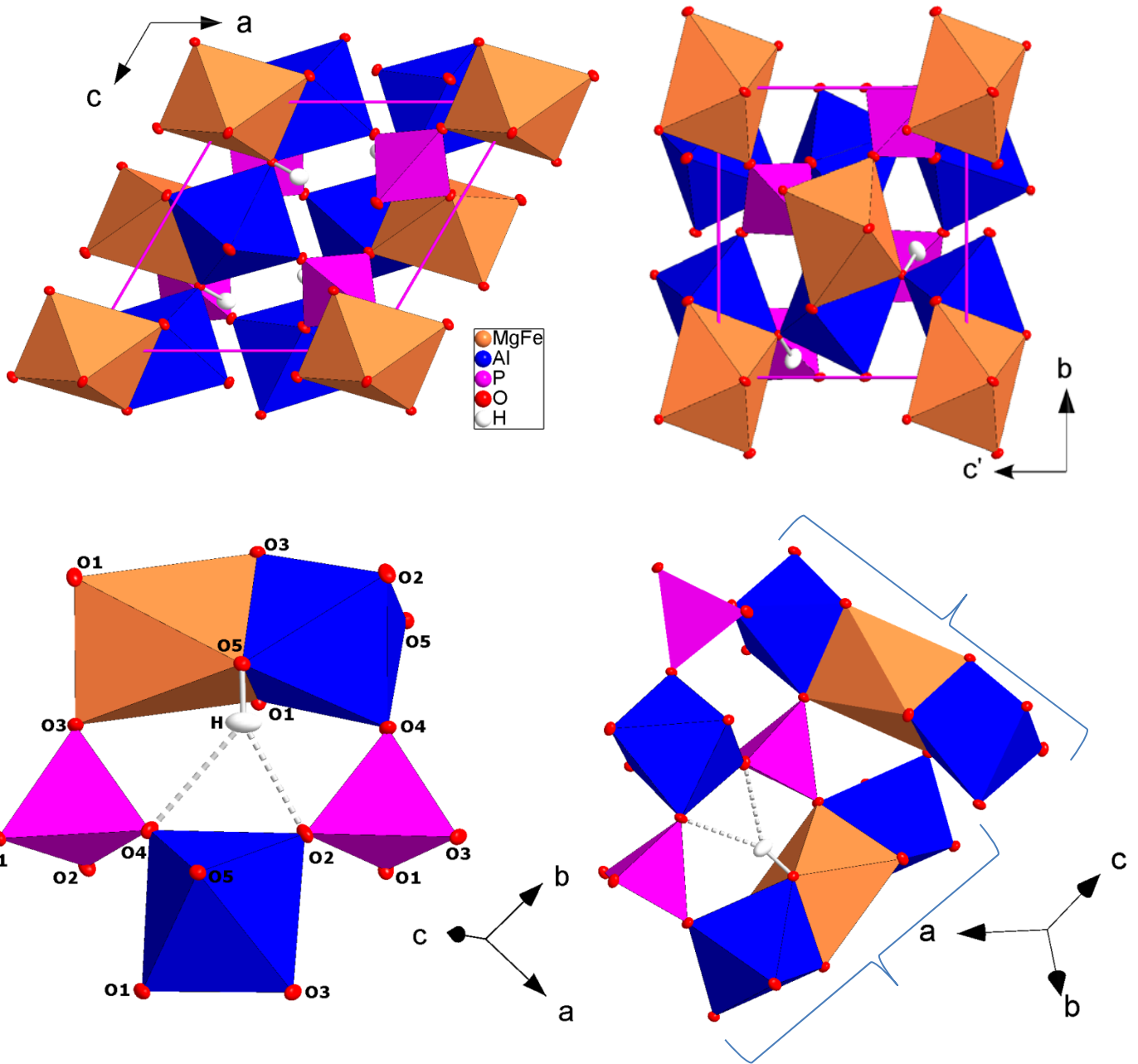
	298 K	3 K
Mg - O1 x 2	2.0181(5)	2.0161(6)
Mg - O3 x 2	2.0807(4)	2.0657(5)
Mg - O5 x 2	2.0882(6)	2.0813(6)
Al - O1	1.9454(7)	1.9347(10)
Al - O2	1.8224(7)	1.8137(10)
Al - O3	1.9366(7)	1.9319(10)
Al - O4	1.8253(8)	1.8239(10)
Al - O5	2.0200(8)	2.0066(11)
Al - O5'	1.9074(8)	1.9000(11)
P - O1	1.5429(5)	1.5389(8)
P - O2	1.5171(6)	1.5125(8)
P - O3	1.5438(6)	1.5412(7)
P - O4	1.5133(6)	1.5121(7)
O5 - H	0.9755(9)	0.9761(11)
O5 - H*	0.9997	0.9968
O5 - H...O2	152.67(9)	152.7(1)
O5...O2	3.014(1)	3.015(1)
H...O2	2.114(1)	2.113(1)
O5 - H...O4	135.73(8)	135.6(1)
O5...O4	3.156(1)	3.135(1)
H...O4	2.383(1)	2.362(1)

\* Bond distance corrected for "riding motion" effect following Busing and Levy (1964)

372  
 373  
 374  
 375  
 376  
 377  
 378  
 379  
 380  
 381  
 382  
 383  
 384  
 385  
 386  
 387  
 388

389  
390  
391  
392  
393  
394  
395  
396

Figure 1. The crystal structure of lazulite, viewed down [010] (*top left*) and [100] (*top right*), and its bifurcated H-bonding scheme (*bottom left*), based on the neutron structure refinement of this study (intensity data collected at 298 K). Displacement ellipsoid probability factor: 50%. In bracket: the triple face-sharing  $\text{Al}_{\text{oct}}(\text{Mg,Fe})_{\text{oct}}\text{-Al}_{\text{oct}}$  building unit (*bottom right*).

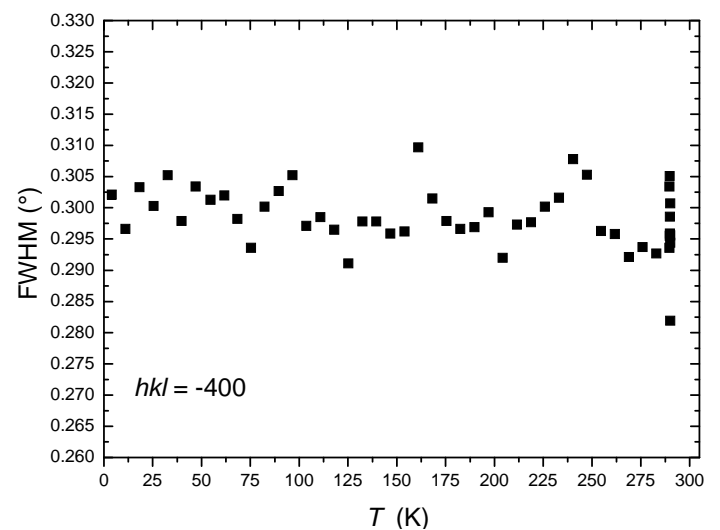
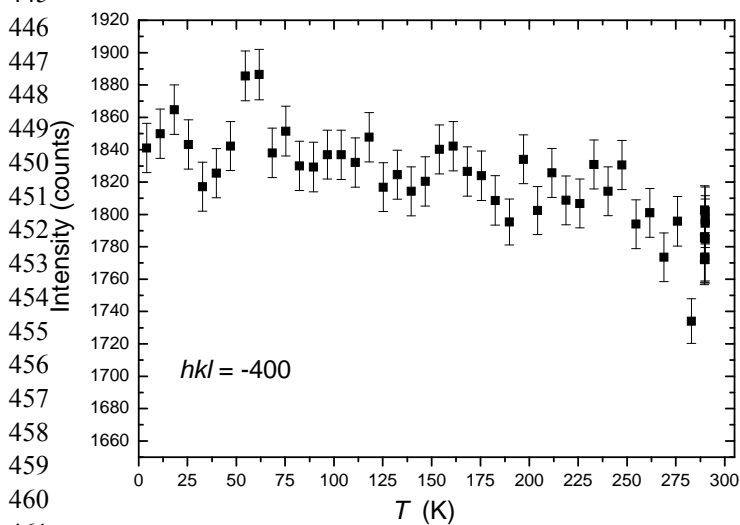
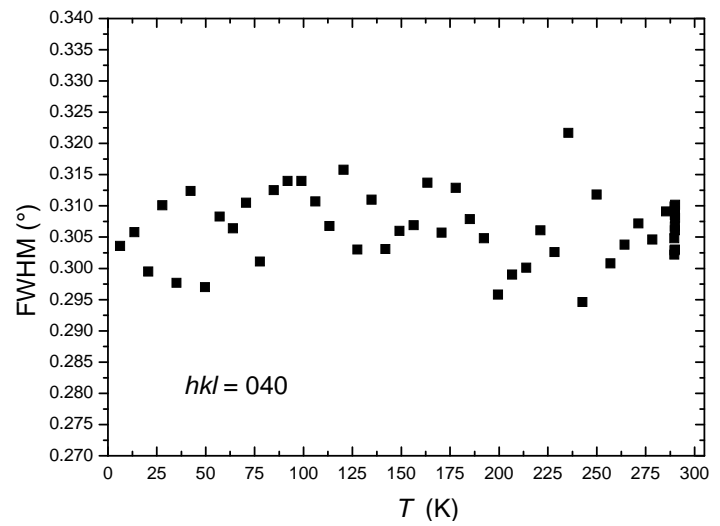
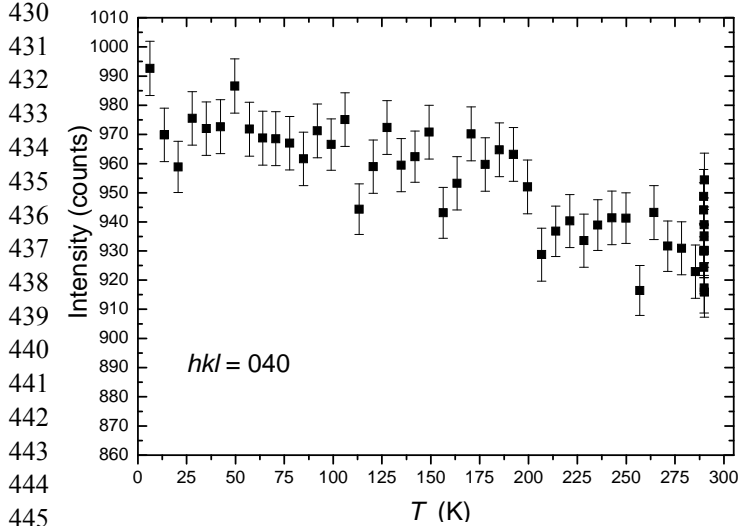
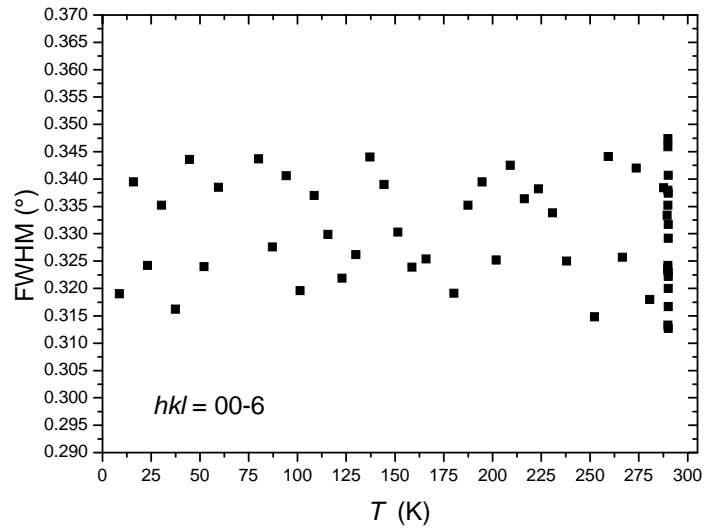
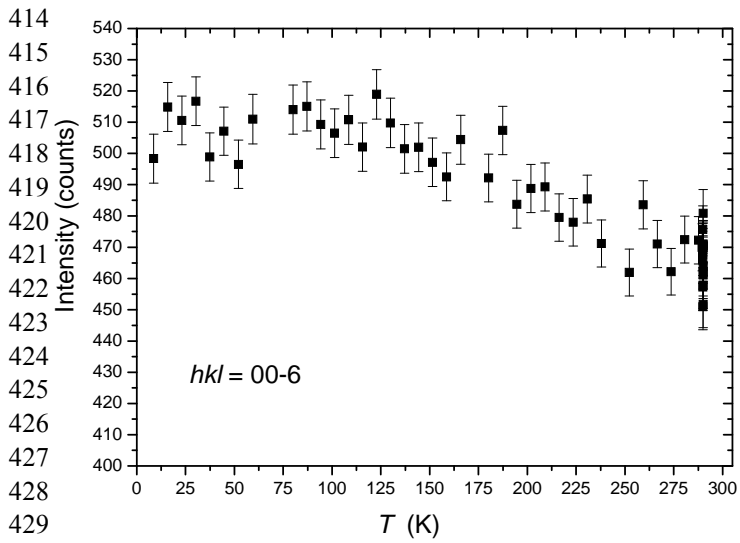


397  
398  
399

400  
401  
402  
403  
404  
405  
406  
407  
408

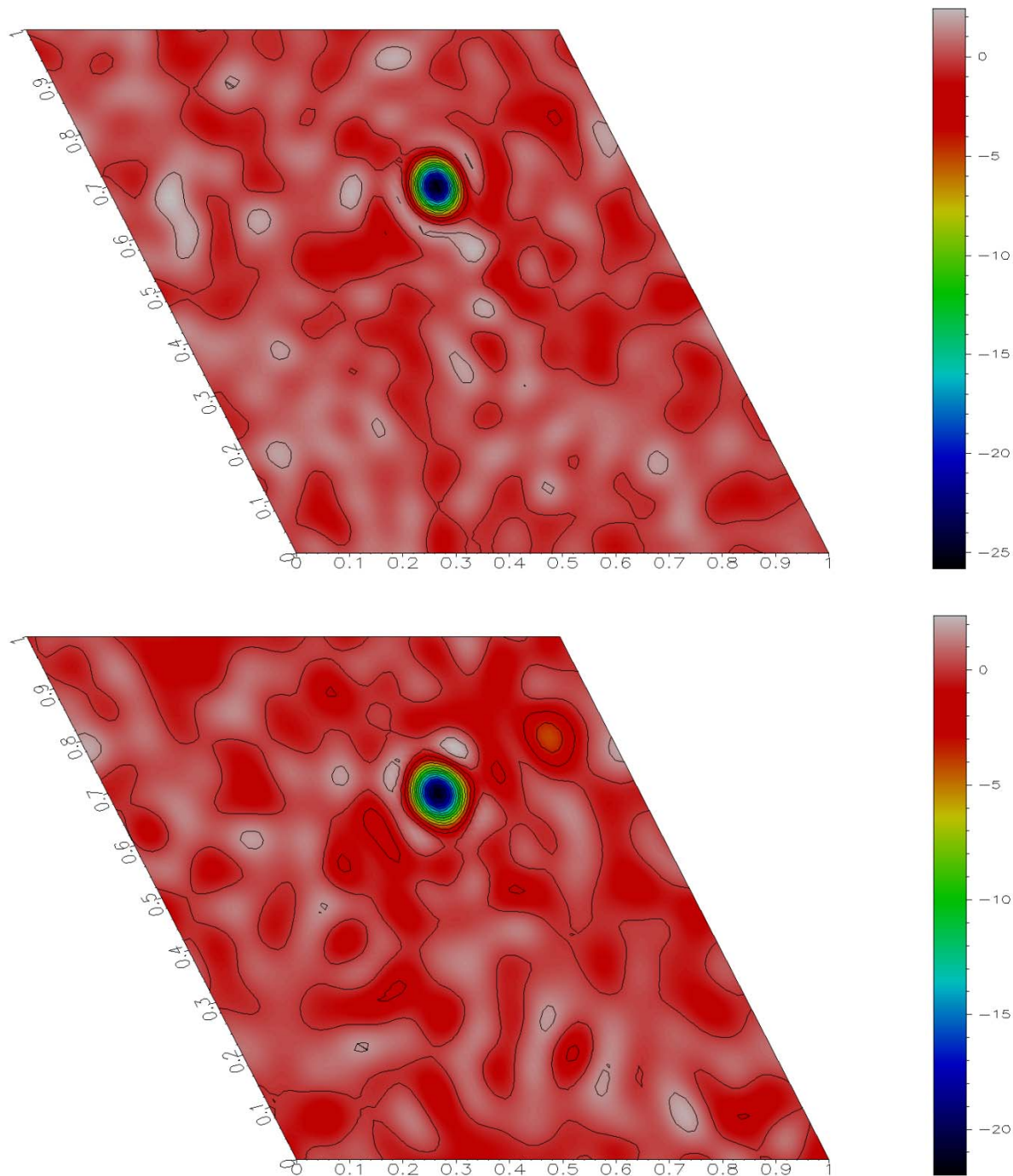
409 Figure 2. Evolution of the integrated intensities and of the full-width-at-half-maxima (FWHM) of  
410 the Bragg reflections 00-6 (top left and right), 040 (mid left and right) and -400 (bottom left and  
411 right) with  $T$ .

412  
413





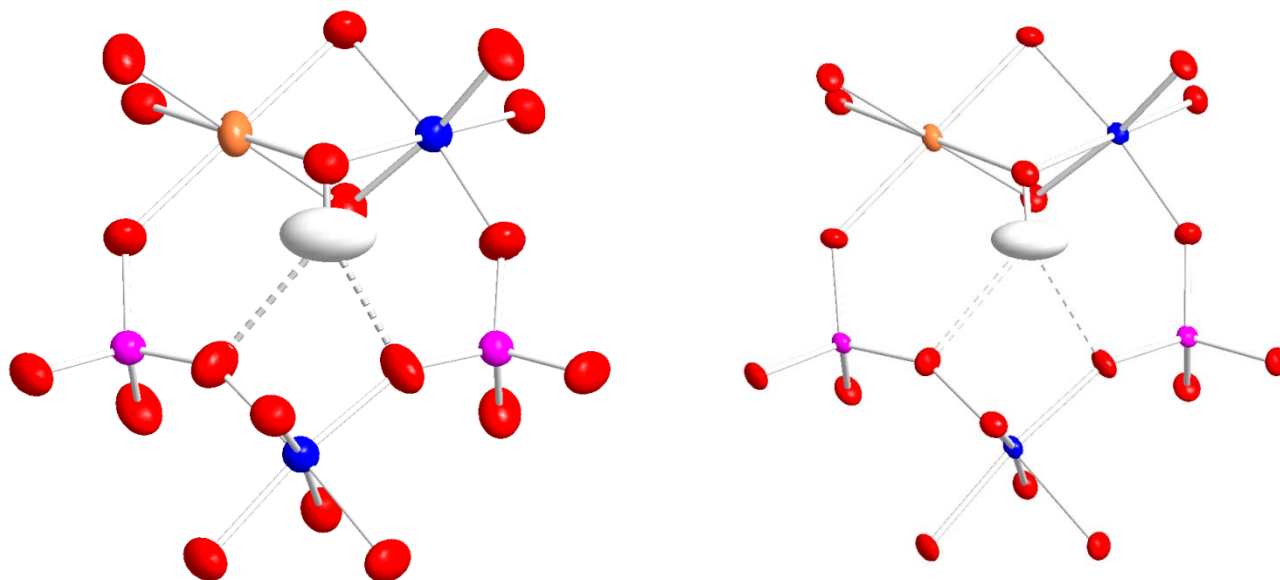
465 Figure 3. Difference-Fourier maps of the nuclear density ( $xy$  sections,  $x$  horizontal;  $z \sim 0.7$ ) at 298 K  
466 (*top*) and at 3 K (*down*), calculated with coefficients  $F_o - F_c$  and phased by  $F_c$ . The  $F_c$  were  
467 calculated from a structural model without the H site. Color bar unit:  $\text{fm}/\text{\AA}^3$ .  
468  
469



470  
471  
472  
473  
474  
475  
476

477  
478  
479  
480  
481  
482  
483  
484  
485

Figure 4. Magnitude of the atomic displacement ellipsoids, with probability factor 99%, based on the structure refinements at 298 K (*left side*) and at 3 K (*right side*). Colors and orientations as in Fig. 1.



486  
487  
488  
489  
490  
491  
492  
493  
494  
495  
496  
497  
498  
499  
500  
501  
502  
503  
504  
505  
506  
507  
508  
509  
510  
511  
512  
513